Thermal stability of resistive switching effect in ZnO/$BiFeO_3$ bilayer structure

Cite as: AIP Advances **9**, 035121 (2019); https://doi.org/10.1063/1.5053577
Submitted: 23 August 2018 . Accepted: 04 March 2019 . Published Online: 13 March 2019

H. Y. Zhang, W. M. Xiong, X. Y. Zhang, Biao Wang, and Yue Zheng

Thermal stability of resistive switching effect in $ZnO/BiFeO_3$ bilayer structure

Cite as: AIP Advances 9, 035121 (2019); doi: 10.1063/1.5053577
Submitted: 23 August 2018 • Accepted: 4 March 2019 •
Published Online: 13 March 2019

H. Y. Zhang,[1,2] W. M. Xiong,[1,2] X. Y. Zhang,[2,3] Biao Wang,[1,3] and Yue Zheng[1,2,a)]

AFFILIATIONS

[1]State Key Laboratory of Optoelectronic Materials and Technologies, School of Physics, Sun Yat-sen University, Guangzhou 510275, China
[2]Micro&Nano Physics and Mechanics Research Laboratory, School of Physics, Sun Yat-sen University, Guangzhou 510275, China
[3]Sino-French Institute of Nuclear Engineering and Technology, Sun Yat-sen University, Zhuhai 519082, China

[a)]**Electronic address:** zhengy35@mail.sysu.edu.cn

ABSTRACT

Superior thermal stability of resistive switching performance is essential for resistive random access memory (R-RAM) device with high reliability. Thermal stable resistive switching performance can be achieved in $ZnO/BiFeO_3$ bilayer structure by modifying the interface. The bilayer structure with a distinct interface is fabricated with an optimized annealing process in chemical solution deposition method. This bilayer structure shows a better thermal stability compared to the case with an indistinct interface. Attempt has been made to explain such effects based on conductive filament mechanism. We propose that the confinement of the oxygen vacancies migration at distinct interface could be the reason for the thermal stability. Our results indicate that morphology of interface is an important factor to improve the thermal stability of R-RAM.

I. INTRODUCTION

Resistive random access memory (R-RAM) of transition metal oxide is one of the most promising candidates to replace flash memories, because of several advantages such as remarkable scalability and good compatibility with CMOS technology.[1–3] Various transition metal oxides, including TiO_2, ZnO and $BiFeO_3$, etc., have been used as the switching layer in R-RAM.[4,5] Nowadays, one of the unresolvable issues of the industrial application of R-RAM is the thermal stability of resistive switching performance.[6] Actually, resistive switching performance, including the uniformity, endurance and retention, is highly sensitive to temperature. For example, Fang et al.[7] studied the $TiN/HfO_x/Pt$ structure and found the non-uniformity of resistive switching performance and the decrease of ON/OFF ratio, when temperature increases. Similarly, such thermal effect was also revealed in $TiN/HfO_2/Ti/TiN$[8] bilayer structure. In addition, retention characteristics in some bilayer structures[9–11] show degradation with the rise of temperature, leading to poor reliability.

Several key factors are responsible for the thermal stability of resistive switching performance, such as materials of the switching layer[12] and the electrode,[13] the oxidation and diffusion of defects within the conductive filament.[14] Recent study found that the retention properties of $ITO/ZrO_2/ITO$ structure could be improved by introducing a $ZrO_2/AlON$ interface at a high temperature of 85 °C.[15] Meanwhile, by introducing such an insert layer (e.g., AlON) into the traditional single layer structure, the resulting bilayer structure could enhance its resistive switching performance, for example, reducing power consumption,[16] improving the switching uniformity[17] and endurance.[18,19] Researchers speculated the interface in R-RAM is probably one of the important factors affecting thermal stability. However, few studies were reported on the effects of interface on thermal stability of resistive switching performance.[20] In this work, we aim to study the thermal stability of the resistive switching by modifying the interface of a bilayer structure.

In this paper, we choose $ZnO/BiFeO_3$ (ZnO/BFO) bilayer structure, which has reproducible and reliable resistive switching characteristics, for the resistive switching device material. The sample is

fabricated using chemical solution deposition method. After modifying the interface using different annealing methods in our experiment, the effect of interface on the thermal stability of resistive switching performance has been analyzed. It is found that a conductive filament mechanism based on the migration of oxygen vacancies is responsible for the thermal stability of resistive switching performance in ZnO/BFO bilayer structure.

II. EXPERIMENT

The ZnO/BFO bilayer films were fabricated on the commercial $Pt/Ti/SiO_2/Si$ substrate using chemical solution deposition method. The fabrication procedure of the bilayer structure is shown as following. The precursor solution of BFO was synthesized by dissolving bismuth nitrate pentahydrate (3.056 g) and iron nitrate nonahydrate (2.424 g) into a mixed solution of 2-methoxyethanol (16 mL), acetic acid (4 mL) and ethanolamine (1 mL). The deposition of the BFO film was carried out by spin-coating at 4000 rpm for 30 s and prefiring at 350 °C for 5 min to remove organics. Then the films were annealed at 600 °C for one hour in the air. Similarly, ZnO precursor solution was prepared by introducing zinc acetate dehydrate (2.915 g) into a mixed solution of methanol (20 mL) and diethanolamine (1 mL). Then, the ZnO solution was spin-coated on BFO layer at 3000 rpm for 40 s and prefired at 310 °C for 5 min. After that, the ZnO/BFO bilayer films were annealed at 600 °C for one hour. Finally, the Au top electrodes with a diameter of 0.3 mm were patterned on the films by electron beam evaporation with a metal shadow mask. Note that, the BFO layer and ZnO layer are annealed independently and subsequently, so to obtain a distinct ZnO/BFO interface in the above procedure. Further, in order to clarify the role played by distinct interlayer on the thermal stability of R-RAM, we fabricate another ZnO/BFO bilayer films with an indistinct ZnO/BFO interface by annealing these two films simultaneously.[21]

After fabrication, the crystallinity and phases of ZnO/BFO bilayer film were characterized by X-ray diffraction (XRD, D-MAX 2200 VPC, Rigaku) with Cu $K\alpha$ radiation (λ = 0.154 nm) operated at 40 kV and 26 mA. The morphology and cross-sectional images were examined by atomic force microscope (AFM, MFP-3D Infinity, Asylum Research) and scanning electron microscopy (SEM, Quanta 250F, FEI), respectively. The chemical states of ions and depth profile of ZnO/BFO bilayer film were analyzed by X-ray photoelectron spectrometer (XPS, ESCA LAB 250Xi, Thermo Fisher). The I-V characteristics were measured by semiconductor characterization system (SCS, Keithley 4200). The current maps of the bilayer structure were measured by conductive AFM (c-AFM).

III. RESULTS AND DISCUSSION

Fig. 1(a) plots the XRD pattern (with the sketch of Au/ZnO/BFO/Pt structure inserted). Fig. 1(b) shows the element distribution along the depth direction using XPS (The depth direction is defined along ZnO/BFO direction, with the sputter time representing the distance from the top of bilayer film). Fig. 1(c) and (d) exhibit ZnO layer surface morphology using AFM and cross-sectional secondary electrons image of ZnO/BFO bilayer films using SEM, respectively. Specifically, the XRD results indicate the presence of wurtzite ZnO and perovskite BFO. The element distribution along the depth direction confirms the existing of a distinct ZnO/BFO interface, which could be also confirmed by the SEM

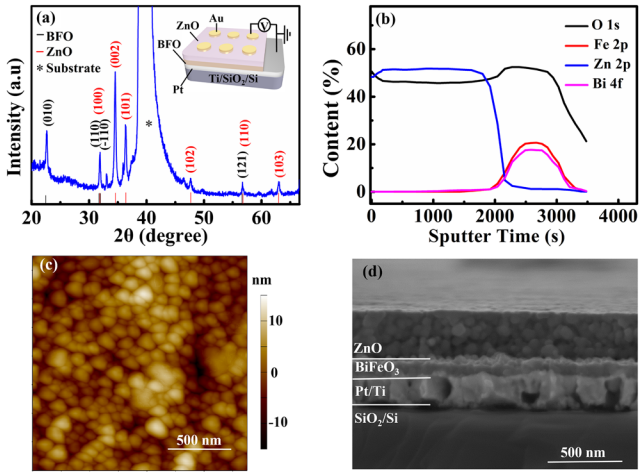

FIG. 1. (a) XRD pattern of ZnO/BFO bilayer film. The inset: schematic diagram of the Au/ZnO/BFO/Pt device and the measuring configuration. (b) The depth-profiling XPS analysis, (c) the morphology and (d) cross-sectional secondary electrons images of ZnO/BFO bilayer film.

image in Fig. 1(d). The ZnO layer surface morphology shows that the grain diameter on the surface is around 40~80 nm. And the cross-sectional secondary electrons image reveals that the ZnO/BFO bilayer is well deposited on the $Pt/Ti/SiO_2/Si$ substrate and the thickness of the films is about 500 nm. From Fig. 1, using the above introducing procedures in Sec. II, the ZnO/BFO bilayer film was successfully fabricated with a distinct ZnO/BFO interface.

Using DC voltage sweep mode at room temperature, the resistive switching characteristics of ZnO/BFO bilayer structure are analyzed, with results plotted in Fig. 2. The forming process is carried out by applying a positive voltage of 7.3 V with the compliance current being 5×10^{-3} A on the Pt electrode to activate the subsequent resistive switching properties, as inserted in Fig. 2(a). Typical bipolar resistive switching characteristics can be reproduced in this bilayer structure for 400 consecutive cycles under the voltage sweep of 0V → 4V → 0V → −1.2V → 0V with the voltage step of 0.01 V. The values of set voltage (V_{set}) and reset voltage (V_{reset}) mainly are within a relatively narrow range, i. e., from 1.9 V to 2.5 V and from -0.6 V to -0.8 V, respectively, as shown in Fig. 2(a). Comparing with BFO and ZnO monolayer structures shown in Fig. S1(a) and (c), resistive switching performance of this bilayer structure has been greatly improved, which exhibits high uniformity and repeatability. Moreover, as shown in Fig. 2(b), the resistance values at high- (HRS) and low-resistance states (LRS) show no significant degradation after 400 switching cycles, and the values of the ON/OFF ratio maintain between 400 and 500. The result of our bilayer structure shows better endurance than those of BFO and ZnO monolayer structures (See in Fig. S1(b) and (d)). Therefore, at room temperature, because of the introduction of ZnO/BFO interface, bilayer structure can indeed improve the resistive switching performance compared with the single layer structure.

In the following, the thermal stability would be examined by varying operating temperatures of this bilayer structure. Firstly, we measured the I-V characteristics of ZnO/BFO bilayer structure at temperatures ranging from 5 °C to 100 °C. Here, for each

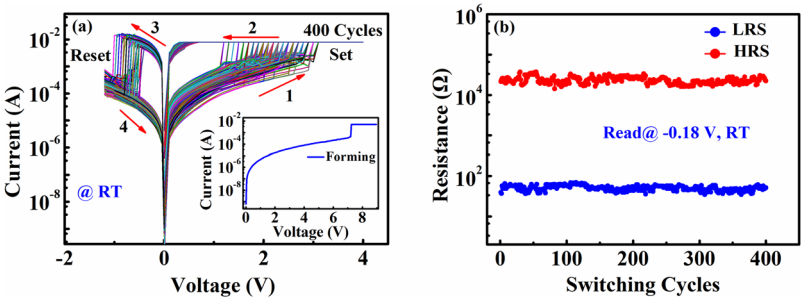

FIG. 2. (a) Bipolar I-V curves with 400 consecutive cycles of ZnO/BFO bilayer structure at room temperature (RT), the inset: forming curve. (b) The resistance evolutions for at high- (HRS) and low-resistance states (LRS) in ZnO/BFO bilayer structure (Read in -0.18 V) at RT.

temperature, the sample was stabilized for half an hour beforehand, then the I-V curves were measured with a compliance current of 5×10^{-3} A more than 60 times, in which the testing time-interval for each cycle was two minutes. As shown in Fig. S2(a)–(e), the V_{reset} and V_{set} at various temperatures applied here are almost the same, which indicates the high stability and uniformity of I-V characteristics. Besides, both V_{set} and V_{reset} are insensitive to temperature varying from 5 °C to 100 °C, as presented in Fig. 3(a). The values of V_{set} and V_{reset} at different temperatures mainly are within a relatively narrow range, i. e., from 1.7 V to 2.7 V and from -0.48 V to -0.8 V, respectively. The resistance values at LRS and HRS obtained from the I-V curves (See in Fig. 3(b)) have no significant degradation after 60 switching cycles, and the resulting high ON/OFF ratio are well maintained. In addition, we also test the retention performance of ZnO/BFO bilayer structure with applied voltage of 0.18 V at 100 °C. As seen in Fig. 3(c), the resistance values at LRS and HRS keep constant within the retention time more than 10^5 s, which confirms the reliability of resistive switching performance in our sample.

The above experimental observations of resistive switching performance, such as uniformity, endurance and retention, indicate clearly a great thermal stability of ZnO/BFO bilayer structure with a distinct interface. For comparison, we fabricated Sample II, another similar sample of ZnO/BFO bilayer structure but with indistinct interface (For detail, see supplementary material 3), and analyzed its thermal stability. In the following, we try to give our mechanistic interpretation of the interface effects on thermal stability.

Comparing to the interface morphology and the profile depth of sample I (Fig. 1(d) and (c)), the cross-sectional secondary electrons image using SEM (see in Fig. S3) and the depth profile using XPS of Sample II (see in Fig. S4(b)) reveal the presence of an indistinct ZnO/BFO diffusion layer, which is believed to be owed to the severe inter-diffusion during the annealing process as mentioned in Sec. II (For detail, see supplementary material). The I-V curves of Sample II at various temperatures presented in Fig. S5 show the strong fluctuation behavior in the switching process (See in Fig. S5(a)–(d)), where the mean values and deviations of V_{set} and V_{reset} are more uncertain with temperature increasing from room temperature to 100 °C (See in Fig. S5(e)). Therefore, the resulting resistance values at LRS and HRS fluctuate at least an order of magnitude at temperatures higher than 50 °C, as shown in Fig. S5(f). In this regard, an indistinct diffusion-interface significantly results in the adverse effects on thermal stability of resistive switching performance at high temperatures.

Theoretically, two mechanisms are widely accepted to interpret the resistive switching performance of R-RAM, i.e., interface-type and filamentary-type, which can be distinguished by the dependence of the resistance on the electrode area. In order to confirm the determinant mechanism in the ZnO/BFO bilayer structure with a distinct interface, we use c-AFM to measure the current map of our sample. The current map with a scanning area of 7.5 × 7.5 μm^2 demonstrates the poor conductivity in as-grown bilayer film (as presented in Fig. 4(a)). Several discontinuous bright spots of large current appear on the scanning area (Fig. 4(b)), after the set process using a positive voltage of 2.3 V, which, however, disappear after the reset process with a negative voltage of -0.7 V. According to the previous studies, these bright spots are associated with the localized conductive regions, suggesting the filamentary-type mechanism responsible for the resistive switching performance in this ZnO/BFO bilayer structure.[22,23]

As known, conductive filament in transition metal oxide could be mainly formed by metal cations or oxygen vacancies.[3,24] In order to get a clear physical picture of the conductive filament in ZnO/BFO bilayer film, we fitted the I-V curves in the double-logarithmic scale for the positive voltage sweep regions to analyze the current conduction mechanism. The results are presented in Fig. 5(a), from which we can see that, for the LRS, the slope of the curves in bilayer structure is closed to 1, showing that the conduction is dominated by Ohmic conduction. On the other hand,

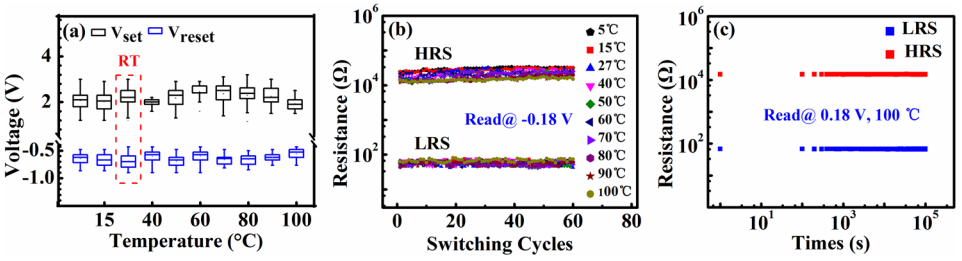

FIG. 3. (a) The distributions of V_{set} and V_{reset} and (b) the resistance evolutions at HRS and LRS (read in -0.18 V) monitored in the temperature range from 5 °C to 100 °C in ZnO/BFO bilayer structure. (c) The retention performance tested at 100 °C with a voltage of 0.18 V in ZnO/BFO bilayer structure.

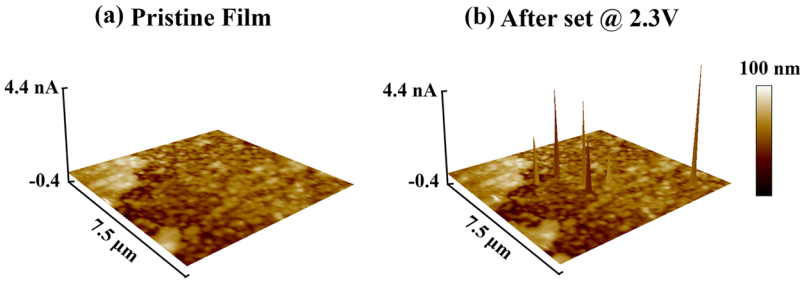

FIG. 4. C-AFM topography images and current maps of ZnO/BFO bilayer film (a) in its initial state and (b) after being set with 2.3 V.

for the HRS, the slope is closed to 1 in low voltage region, while obviously greater than 1 in relatively high voltage region. This is a typical space-charge-limited current (SCLC) conduction mechanism with traps.[25,26] Further, in low voltage region, since the concentration of the thermally generated free carriers is larger than that of injected carriers, the current behavior will exhibit Ohmic conduction ($I \propto V^m$, m ≈ 1). In high voltage region, the density of injected carriers is larger than that of the thermally generated free carriers and the conduction is controlled by traps, leading to the nonlinear I–V relation ($I \propto V^m$, m > 1). The chemical state of elements in the ZnO/BFO bilayer structure analyzed by XPS could help us to clarify the type of traps. Fig. 5(b) and (c) show the oxygen compositions of ZnO and BFO layers, respectively. We can see that the binding energies of the O 1*s* peaks at ~530.0 eV and ~299.8 eV are owing to the O^{2-} ions, while the higher energies at ~530.4 eV and ~530.3 eV correspond to the oxygen vacancies in ZnO layer and BFO layer.[27,28] The amount of oxygen vacancies (proportional to the integration area of the corresponding curve shown in Fig. 5(b)) in BFO layer is significantly larger than that in ZnO layer. This can be further confirmed by the Fe 2*p* spectra. As shown in Fig. 5(d), there are two broad peaks, corresponding to Fe

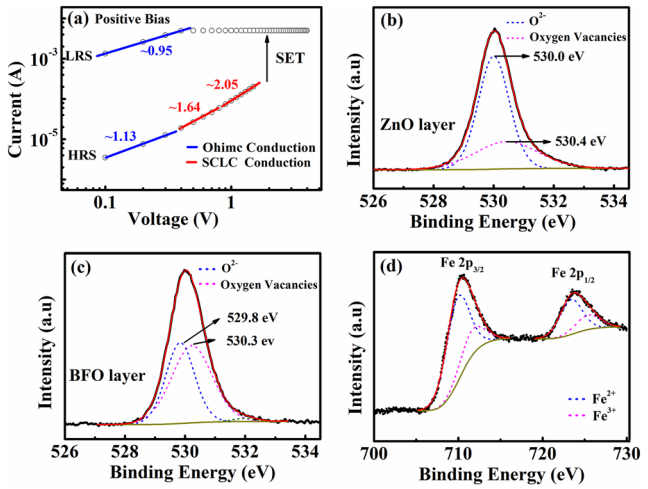

FIG. 5. (a) The fitted I-V curves in double-logarithmic scale of ZnO/BFO bilayer structure in positive voltage sweeps. Red: space-charge-limited current (SCLC) conduction in HRS. Blue: linear Ohmic conduction in LRS and HRS. The O 1*s* XPS spectra of (b) ZnO layer and (c) BFO layer. (d) The XPS spectrum of Fe 2*p* in ZnO/BFO bilayer film.

$2p_{1/2}$ and Fe $2p_{3/2}$ states. After fitting the resulting peaks, it is found that the peaks of Fe^{2+} $2p_{3/2}$ and Fe^{2+} $2p_{1/2}$ are located in 709.9 eV and 723.4 eV respectively while the Fe^{3+} $2p_{3/2}$ and Fe^{3+} $2p_{1/2}$ are in 711.6 eV and 725.4 eV, demonstrating the coexistence of Fe^{2+} and Fe^{3+} valence states. According to the defect chemistry, the transformation from Fe^{3+} to Fe^{2+} is attributed to charge compensation of oxygen vacancies.

Based on the aforementioned experimental observations and analysis, the formation and rupture of conductive filament mechanism could explain resistive switching behavior of ZnO/BFO bilayer structure. During the forming process, the oxygen vacancies migration from BFO layer to ZnO layer under the positive voltage bias is easily confined by the ZnO/BFO interface due to the existence of traps. When the applied positive voltage bias is sufficient large, the oxygen vacancies could migrate to cathode and form a conductive filament, resulting in a sharp increase of current and the transition of this bilayer structure from HRS to LRS. According to previous works,[29] the cross-section of the conductive filament is determined by the concentration of oxygen vacancies. Thus, the conductive filaments with large cross-section are easily formed in the BFO layer because of the presence of large amount of oxygen vacancies. Before the applied positive voltage sweeps back to 0V, oxygen vacancies still move toward and continuously accumulate at the cathode, leading to a large current in that local region (Fig. 4(b)). During the reset process, the oxygen vacancies are dragged back to anode under the reverse voltage bias. Oxygen vacancies in ZnO layer cannot easily pass through the interface due to the interfacial confinement effects and they will accumulate in the vicinity of interface under the low reverse voltage. On the other hand, the oxygen vacancies in BFO layer are dragged back to anode, giving rise to the rupture of conductive filament near the interface and switch the structure to the HRS (Fig. 6(a)). When the positive voltage bias is applied to the structure again, oxygen vacancies will move to the cathode with the increase of positive voltage bias and repair the conductive filament (Fig. 6(b)). Therefore, the formation and rupture of conductive filament are constrained at the ZnO/BFO interface.

Because of the presence of large number of traps in the ZnO/BFO distinct interface, it requires a sufficient high temperature fluctuation for the oxygen vacancies de-trapped out to participant the formation and rupture process of conductive filament. Therefore, as experimental observed, the resistive switching performance is thermal stable in the temperature ranging from 5 °C to 100 °C (See in Fig. 6(a) and (b)). On the contrary, there are not so many traps found in indistinct diffusion interface in Sample II of the bilayer structure, the oxygen vacancies migration, which is sensitive to the temperature, leads to the frequent

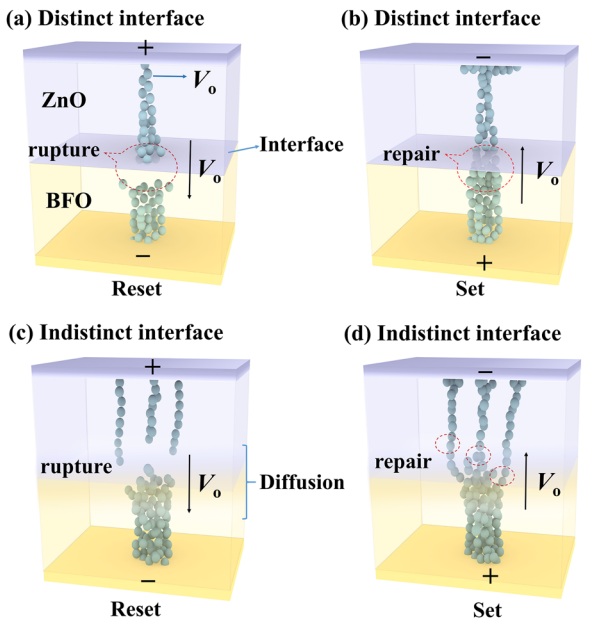

FIG. 6. Schematic description of the conduction mechanism (a) reset process and (b) set process for ZnO/BFO bilayer structure with a distinct interface, and (c) reset process and (d) set process for Sample II.

formation and rupture processes of conductive filament, thus a thermal instability of resistive switching performance, as shown in Fig. 6(c) and (d). Moreover, the number of conductive filament in the case of indistinct interface is quite larger than that in the case of distinct interface, which enhances such thermal instability of resistive switching performance via conductive filament mechanism (See in Fig. 6(c) and (d)).

IV. CONCLUSIONS

In summary, we fabricated a ZnO/BFO bilayer structure with a distinct ZnO/BFO interface on Pt/Ti/SiO_2/Si substrate using chemical solution deposition method. It shows excellent resistive switching performance with a high ON/OFF ratio, great endurance, stability over temperature range from 5 °C to 100 °C, and no degradation of data retention at 100 °C (>10^5 s). By comparing with the thermal stability of resistive switching performance in another ZnO/BFO bilayer structure with an indistinct interface, it is found that the distinct ZnO/BFO interface contribute to obtain good thermal stability. The current maps measured by c-AFM demonstrate the filamentary nature of resistive switching performance. Analyses of current conduction and element distribution along the depth profile of the bilayer film using XPS indicate that the migration of oxygen vacancies in BFO plays an important role in the formation and rupture of conductive filament. Therefore, a conductive filament mechanism based on the migration of oxygen vacancies is suggested to explain the effect of interface on thermal stability. Due to the presence of distinct interface, large amount of oxygen vacancies are easily trapped in the distinct interface and hardly de-trapped by thermal assistance, thus there are not so many oxygen vacancies could take part in the formation and rupture of conductive filament. In this regard, the number and morphology of conductive filament responsible for resistive switching performance could keep stable in the condition of large temperature fluctuation, which, equivalently, a thermal stability of resistive switching performance in a wide range of temperature as observed in our experiment. Our result can help to understand the effect of modification of interface on thermal stability of R-RAM.

SUPPLEMENTARY MATERIAL

See supplementary material for Fig. S1–S5 and the fabrication procedure of ZnO/BFO bilayer structure with an indistinct interface.

ACKNOWLEDGMENTS

The authors gratefully acknowledge the financial support from the NSFC (Nos. 11402312, 11474363, 11672339), the Guangdong Natural Science Funds (No. 2015A030313082), the Guangzhou Science and Technology Project (No. 201707020002), Fok Ying Tung Foundation, Science and Technology Innovation Project of Guangdong Provincial Education Department and Guangdong Natural Science Funds for Distinguished Young Scholar.

REFERENCES

[1] H. S. P. Wong, H. Y. Lee, S. Yu, Y. S. Chen, Y. Wu, P. S. Chen, B. Lee, F. T. Chen, and M. J. Tsai, P. IEEE. **100**(6), 1951 (2012).
[2] A. Sawa, Mater. Today. **11**(6), 28 (2008).
[3] D. S. Jeong, R. Thomas, R. S. Katiyar, J. F. Scott, H. Kohlstedt, A. Petraru, and C. S. Hwang, Rep. Prog. Phys. **75**(7), 076502 (2012).
[4] F. Pan, S. Gao, C. Chen, C. Song, and F. Zeng, Mater. Sci. Eng., R. **83**, 1 (2014).
[5] G. Kolhatkar, F. Ambriz-Vargas, B. Huber, R. Thomas, and A. Ruediger, Cryst. Growth. Des. **18**(3), 1864 (2018).
[6] D. Ielmini, Semicond. Sci. Technol. **31**(6), 063002 (2016).
[7] Z. Fang, H. Y. Yu, W. J. Liu, Z. R. Wang, X. A. Tran, B. Gao, and J. F. Kang, IEEE. Electron. Device. Letters. **31**(5), 476 (2010).
[8] C. Walczyk, D. Walczyk, T. Schroeder, T. Bertaud, M. Sowinska, M. Lukosius, M. Fraschke, D. Wolansky, B. Tillack, E. Miranda, and C. Wenger, IEEE. Trans. Electron. Devices. **58**(9), 3124 (2011).
[9] J. Lee, E. M. Bourim, W. Lee, J. Park, M. Jo, S. Jung, J. Shin, and H. Hwang, Appl. Phys. Lett. **97**(17), 172105 (2010).
[10] J. Y. Kwon, J. H. Park, and T. G. Kim, Appl. Phys. Lett. **106**(22), 223506 (2015).
[11] L. Fu, Y. Li, G. Han, X. Gao, C. Chen, and P. Yuan, Microelectron. Eng. **172**, 26 (2017).
[12] S. R. Mohapatra, T. Tsuruoka, K. Krishnan, T. Hasegawac, and M. Aono, J. Mater. Chem. C. **3**(22), 5715 (2015).
[13] B. Traoré, P. Blaise, E. Vianello, L. Perniola, B. D. Salvo, and Y. Nishi, IEEE Trans. Electron. Devices. **63**(1), 360 (2016).
[14] C. H. Kim, H. B. Moon, S. S. Min, Y. H. Jang, and J. H. Cho, Solid. State. Commun. **149**(39), 1611 (2009).
[15] T. L. Tsai, H. Y. Chang, J. J. C. Lou, and T. Y. Tseng, Appl. Phys. Lett. **108**(15), 153505 (2016).
[16] Y. Bai, H. Wu, Y. Zhang, M. Wu, J. Zhang, N. Deng, H. Qian, and Z. Yu, Appl. Phys. Lett. **102**(17), 173503 (2013).
[17] R. Huang, X. Yan, K. A. Morgan, M. D. B. Charlton, and C. H. Groot, J. Phys. D: Appl. Phys. **50**(17), 175101 (2017).
[18] M. Lee, C. B. Lee, D. Lee, S. R. Lee, M. Chang, J. H. Hur, Y. B. Kim, C. J. Kim, D. H. Seo, S. Seo, U. I. Chung, I. K. Yoo, and K. Kim, Nature. Mater. **10**(8), 625 (2011).
[19] C. Y. Huang, C. Y. Huang, T. L. Tsai, C. A. Lin, and T. Y. Tseng, Appl. Phys. Lett. **104**(6), 062901 (2014).

[20]I. Valov, Semicond. Sci. Tech. **32**(9), 093006 (2017).
[21]W. J. Ma, W. M. Xiong, X. Y. Zhang, Y. Wang, H. Y. Zhang, C. Q. Wang, B. Wang, and Y. Zheng, Appl. Phys. A-Mater. **122**(4), 337 (2016).
[22]X. Zhu, W. Su, Y. Liu, B. Hu, L. Pan, W. Lu, J. Zhang, and R. Li, Adv. Mater. **24**(29), 3941–3946 (2012).
[23]J. Shang, G. Liu, H. Yang, X. Zhu, X. Chen, H. Tan, B. Hu, L. Pan, W. Xue, and R. Li, Adv. Funt. Mater. **24**(15), 2171 (2014).
[24]R. Waser and M. Aono, Nature. Mater. **6**(11), 833 (2007).
[25]M. A. Lampert, Phys. Rev. **103**(6), 1648 (1956).
[26]J. F. Scott, C. A. Araujo, B. M. Melnick, L. D. McMillan, and R. Zuleeg, J. Appl. Phys. **70**(1), 382 (1991).
[27]J. C. Dupin, D. Gonbeau, P. Vinatier, and A. Levasseur, Phys. Chem. Chem. Phys. **2**(6), 1319 (2000).
[28]T. Yamashita and P. Hayes, Appl. Surf. Sci. **254**(8), 2441 (2008).
[29]M. H. Lin, M. C. Wu, C. Y. Huang, C. H. Lin, and T. Y. Tseng, J. Phys. D: Appl. Phys. **43**(29), 295404 (2010).